THE PENNSYLVANIA STATE UNIVERSITY
SCHREYER HONORS COLLEGE

DEPARTMENT OF ELECTRICAL ENGINEERING

TRANSCOSTAL PHASED-ARRAY REFOCUSING USING ITERATIVE SPARSE OPTIMIZATION AND THE SEMIDEFINITE RELAXATION METHOD

DANIEL F. MCMAHON
FALL 2017

A thesis
submitted in partial fulfillment
of the requirements
for a baccalaureate degree
in Electrical Engineering
with honors in Electrical Engineering

Reviewed and approved* by the following:

Mohamed Almekkawy
Assistant Professor of Computer Science and Engineering
Thesis Supervisor

Julio Urbina
Associate Professor of Electrical Engineering
Honors Adviser

*Signatures are on file in the Schreyer Honors College.

Abstract

Administration of High Intensity Focused Ultrasound (HIFU) treat to tumors in organs shadowed by the ribs is challenging because the ribs absorb ultrasound beams' energy causing the temperature of the ribs to rise, while also distorting the beams, and limiting the focal heat deposition. As a result, the ribs necessitate the continued development of novel focusing algorithms that seek to address the difficulties that they present. In this paper, a new approach that iteratively removes transducer elements is introduced. The method builds on the Limited Power Deposition (LPD) method, which utilized Semidefinite Relaxation (SDR) as a means of relaxing otherwise nonconvex constraints into convex form. The method discussed in this paper iteratively induces sparsity using the one-norm squared as a convex surrogate for the zero-norm. A 1-MHz spherical phased-array is focused onto a target in an inhomogeneous medium in simulations to test the algorithms efficacy. The results of focusing the array with the suggested algorithm are compared to the ray tracing (shadowing) approach. The movement of the waves as they traveled from the array towards the target was modeled using a finite difference time domain propagation model. Temperature simulations that utilized the inhomogeneous Bioheat Transfer Equation (BHTE) were used to determine the temperature rise profile within the Region of Interest (ROI). These simulation results illustrate the benefits of the optimization based approach proposed in this paper over other sparse methods, such as the shadowing method. Accordingly, it is possible to retain the advantages that accompany sparse algorithms, like the shadowing method, without having as large of an impact on focal power deposition. For example, the shutoff transducers could be used for other purposes, such as motion tracking and subsequent refocusing. Due to the ribs' influence on the ultrasound beam, the focal power deposition is lessened, and as a result, treatment times are increased. Due to the increased duration of treatment, considering the ROI to be static may lessen treatment efficacy. Thus, motion tracking would allow treatments of organs, such as the liver, that are both obscured by the ribs and constantly moving to be more effective. Alternatively, in situations where power conservation is essential, like field treatment administration, then elimination of transducers can act as a means of eliminating unnecessary power consumption.

Table of Contents

List of Figures

Chapter 1

Introduction

Improvements in real-time imaging techniques and transducer technologies have enabled HIFU to continue to gain traction as a noninvasive means of treating accessible tumors. As HIFU begins to become more popular, groups have started work on new focusing methods that seeks to maximize the potential of phased-arrays. Examples of this include the work done by Tempany [1] and Sanghvi [2] who using MRI and focused ultrasound as means of guiding HIFU treatment, respectively. Due to continued advances, readily accessible targets, such as the uterine fibroid, have been treated with currently available systems, using both ultrasound and MRI guidance [3].

Targets that are unobscured by the ribs are accessible to treatments using appropriately configured transducers. However, targets shadowed by the ribs, such as the liver, are more difficult to target. The ribs cause abberations and attenuation of the ultrasound beam, as well as an increased risk of burns developing on the overlying skin [4]. One method of dealing with the challenges presented by the ribs is to shut off the elements directly shadowed by them from the perspective of the target. In this approach, known as the shadowing approach, the focusing problem enjoys the benefit of less complexity as a result of the preset sparsity [5]. While this approach was reasonable for arrays capable of producing only pulses in phase with each other, Ebbini *et al.* showed that the use of phased-arrays enables the use of constructive and destructive interference, allowing the treatment to conform to the geometry of the ROI. Phased-arrays allow critical points to be identified. The ability to define critical points led to the virtual array approach. In this approach, the regions between the the ribs, the intercostals, are treated as a virtual array of transducers [6]. The focusing is then done in two steps. During the first step, the virtual array is focused onto the target. In the subsequent step, the physical array is focused so that the requisite excitation in the plane of the virtual array is achieved [6].

In [7], experimental verification of transcostal focusing techniques that utilized time-reversal techniques described in [8–13] was provided. In [14, 15] the problem of transcostal focusing was also studied. There, the effects of the ribs on the ultrasonic beams were investigated by Gelat. The

previously described effects of diffraction [14, 15] were examined by Bobkova, who determined that accounting for them provides advantages over a geometric ray tracing approach. They found an increase in focal power deposition that was accompanied by a large reduction in power losses to the ribs [16]. Together, these studies demonstrate that using an optimization based approach that accounts for the consequences of the ribs provides a more effective treatment than intuitive, geometry based, focusing methods.

The goal of this paper will be building off of the LPD method [17], as was done in [18] by both noniterativly and iteratively inducing sparsity. This paper differs from the previous work in two ways. First, it introduces an iterative approach for HIFU element selection. Second, it modifies the parameters of the constraints defining the solution set to allow for a slightly higher rib power deposition, leading to greater sparsity. The motivation for seeking sparsity is to free ineffective HIFU transducer elements for parallel use in applications such as imaging during treatment. By using an optimization based approach [19] for element selection, a subset that better protects the ribs and heats the target will be selected. Sparsity will be induced by using the one-norm squared as a convex proxy for the zero-norm, a nonconvex function [20]. A consequence of replacing the zero-norm with the one-norm squared, which punishes high magnitude transducer excitations, is the solution is no longer a minimum power solution [20]. To counteract this, it is necessary to first induce sparsity, and then conduct the original optimization problem, using only the subset of elements that remained after sparsity induction. Limiting the transducer quantity will provide three benefits. First, it will lower the chance of the patient developing burns on the skin near the transducers during the administration of the treatment. Second, the total array power expenditure will be reduced. Finally, it will allow the transducers no longer being used for HIFU treatment to be used for other processes, like imaging, in parallel with the treatment.

Chapter 2

Problem Statement

2.1 Limited Power Deposition (LPD) Method

The MPD method [21], [22], [17] finds the solution that minimizes the power deposited across the ribs by examining the set of perspective solutions that deliver adequate focal heating by using convex optimization. During focusing, the optimization problem minimizes the power deposition across the critical points by utilizing interference, while still achieving a prescribed minimum intensity at the focus. To achieve this, the convex optimization problem describing the MPD method minimizes an objective function that is proportional to the sum of heat depositions on each of the critical rib points, while also satisfying a constraint that demands a requisite power deposition at the target(s). The LPD method built upon the MPD method by placing constraints limiting the power deposited upon the ribs. The important distinction between the two methods is that LPD method does not penalize power depositions upon the ribs that are under a certain threshold. As a result, transducer alignments that offer higher therapeutic gains than the solution provided by the MPD method, but that were penalized for exposing the ribs to an innocuous amount of power deposition, are considered. Accordingly, the LPD method is able to find a focusing arrangement with a higher treatment efficacy than the MPD method. In the problem statement of the LPD method, the total power deposited upon the ROI, rather than the power deposited upon the ribs, is considered for minimization. For a transducer array consisting of N elements being focused on L target points, the method can be described by [17]:

$$\begin{aligned} \min_{\mathbf{u}\in\mathbb{C}^N} \quad & ||\mathbf{u}||_2^2 \\ \text{s.t.}: \quad & |\mathbf{u}^{\mathcal{H}}\mathbf{h}_{ti}|^2 \geq \mathbf{p}_{ti}, \quad i = 1,\ldots,L \\ & |\mathbf{u}^{\mathcal{H}}\mathbf{h}_{rj}|^2 \leq \mathbf{p}_{rj}, \quad j = 1,\ldots,M \end{aligned} \tag{2.1}$$

Here, $\mathbf{h}_{ti}$ and $\mathbf{h}_{rj}$ are the $N \times 1$ complex directivity vectors that describe the propagation of the ultrasound waves from the transducers to the target and rib points, respectively. The directivity vectors account for the attenuation and scattering of the waves that occur due to the presence of the inhomogeneities within the ROI. These vectors contain all the information that is necessary to describe the relationship between exciting each transducer element and the subsequent heating of each of the critical and target points. $\mathbf{p}_{ti}$ and $\mathbf{p}_{rj}$ are the requisite power at the targets and the highest allowable power at the rib points, respectively. Additionally, i has values $\{1, ..., L\}$, and j has values $\{1, ..., M\}$. These values represent the L target points and M rib points within the ROI [17]. The set of excitation vectors that satisfy the constraints of the LPD problem can be described as the intersection of the exteriors of L co-centred ellipsoids and the interiors of M co-centered ellipsoids [23]. Depending on the demands laid out by the constraints of the LPD problem, the solution set may be empty.

Inspection of the objective function and the constraints of this optimization problem reveals that both are in quadratic form [17]. Accordingly, this problem falls into a class of problems known as quadratic constraints quadratic programming (QCQP) [24], [25]. The first set of constraints are concave homogenous quadratic constraints, making the problem NP-hard (nondeterministic polynomial time) [26]. The nonconvexity occurs because the set of points described by the set of concave constraints is nonconvex. As a result the problem is unable to be solved using convex optimization techniques. Further adding to the difficulty of solving this problem for real applications is the fact that it assumes prior knowledge of the directivity vectors describing the propagation of the ultrasound waves from the transducers to the targets and the ribs, denoted h_{ti} and h_{rj}, respectively. However, these directivity vectors must first be acquired through direct measurement [27], computational modeling [12], [28], [29], or estimations from the beamforming parameters used in forming single transmit focus (STF) or synthetic aperture (SA) imaging [21].

2.2 Semidefinite Relaxation Approximation

The LPD problem in its current is NP-hard. This is due to the concavity of the first set of constraints. However, it can be relaxed into convex form by using semidefinite relaxation [26], [30]. The approximation relies upon the following identities: $||\mathbf{u}||_2^2 = tr(\mathbf{u}\mathbf{u}^{\mathcal{H}})$, $|\mathbf{u}^{\mathcal{H}}\mathbf{h}|^2 = tr(\mathbf{h}\mathbf{h}^{\mathcal{H}}\mathbf{u}\mathbf{u}^{\mathcal{H}})$, $\mathbf{Q}_i = \mathbf{h}_{ti}\mathbf{h}_{ti}^{\mathcal{H}}$, $\mathbf{F}_j = \mathbf{h}_{rj}\mathbf{h}_{rj}^{\mathcal{H}}$, and $\mathbf{A} \triangleq \mathbf{u}\mathbf{u}^{\mathcal{H}}$. The problem can now be expressed as:

$$
\begin{aligned}
\min_{\mathbf{A}\in\mathbb{C}^{N\times N}} \quad & tr(\mathbf{A}) \\
\text{s.t.}: \quad & tr(\mathbf{A}\mathbf{Q}_i) \geq \mathbf{p}_{ti}, \quad i = 1, \ldots, L \\
& tr(\mathbf{A}\mathbf{F}_j) \leq \mathbf{p}_{rj}, \quad j = 1, \ldots, M \\
& \mathbf{A} \succcurlyeq 0, \\
& rank(\mathbf{A}) = 1
\end{aligned}
\tag{2.2}
$$

The objective function and inequality constraints are now linear functions of A. The set of symmetric positive semidefinite matrices is also convex [26], [31]. However, the rank constraint on A is not convex, and so it must be discarded in order to relax the problem into convex form. The removal of the rank constraint will enable the problem to be solved using an interior points method [19], [25].

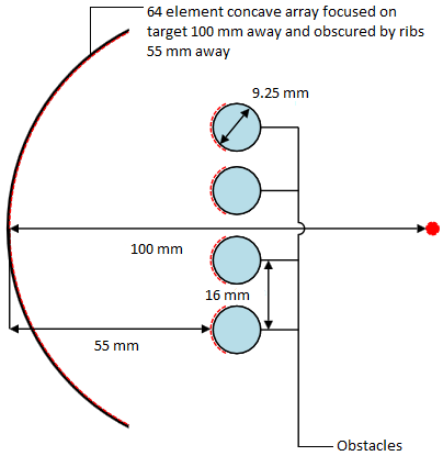

Figure 2.1: Geometry of the region of interest.

Removing the constraint on the rank of A introduces two possible scenarios. The rank of A can either be equal to 1, or it can be greater than 1. In the former case, the relaxed problem is equivalent to the original problem. In order to convert the solution for the relaxed problem to a solution to the original problem, singular value decomposition is performed on A, and the eigenvector corresponding to the only nonzero eigenvalue is used to solve the original LPD problem. In the latter case, the problem differs from the original LPD, and the solution must be converted into one that can satisfy the original problem using randomization techniques [17], [26]. Out of the perspective excitation vectors yielded by the randomization techniques, the one corresponding to the minimum magnitude excitation vector is selected. This vector is then compared to the $\geq$ constraints. In the event that any of these constraints are violated, the vector is scaled up until it satisfies all $\geq$ constraints. The $\leq$ constraints are then checked. If any of them are violated, the solution vector is discarded, and a new one is obtained by performing another round of randomization. This process is conducted until a vector that satisfies all constraints is obtained.

2.3 Relaxation of Noniterative Sparsity Inducing Terms

This paper seeks to utilize sparsity inducing techniques introduced in [20] to reduce the number of elements used during the treatment. This could be done by adding the product of a scalar multiplier, λ, and the zero-norm of A, $\|A\|_0$, to the objective function. This would allow the number of elements of A to be counted, and the penalty for each nonzero element to be modified by manipulating λ. However, the presence of the zero-norm is not convex, so the problem would be NP-hard. Thus, solving it would entail an exhaustive search of all possible transducer combinations that are capable of satisfying the constraints [32]. Doing this would result in the objective function:

$$\min_{\mathbf{u}\in\mathbb{C}^N} \quad ||\mathbf{u}||_2^2 + \lambda||\mathbf{u}||_0 \tag{2.3}$$

For an array of 64 elements, this would require intense computational input, and as a result is undesirable. Thus, it is desired to instead arrive at a near optimal solution, by approximating the

objective function into a form that can efficiently be solved. Instead of the zero-norm, the one-norm, denoted by $\|\,.\,\|_1$, is commonly used as a convex surrogate [33]. However, the one-norm, despite being the closest convex approximation of the zero-norm, is a surrogate that suffers from being weaker both in terms of measuring and inducing sparsity [33]. Unlike the zero-norm, the one-norm also accounts for the magnitude of each nonzero element, giving additional penalty to large elements. By using the one-norm as an approximation for the zero-norm, the objective function can now be rewritten as:

$$\boxed{\min_{\mathbf{u}\in\mathbb{C}^N} \quad ||\mathbf{u}||_2^2 + \lambda||\mathbf{u}||_1} \tag{2.4}$$

However, it can be shown, as was done in [20], that this objective function can be reparameterized to:

$$\boxed{\min_{\mathbf{u}\in\mathbb{C}^N} \quad ||\mathbf{u}||_2^2 + \lambda'||\mathbf{u}||_1^2} \tag{2.5}$$

Here, λ' is a scaled version of λ, allowing the same optimal solution to be reached with the inclusion of the one-norm squared in the objective function. Using the one-norm squared will allow the objective function to more easily be relaxed into convex form [20]. Accordingly, the one-norm squared penalty is utilized during sparsity induction. In order to alter the one-norm squared constraint, the following equalities are initially utilized [32]:

$$\boxed{\begin{aligned} ||\mathbf{u}||_1^2 = (\sum_{n=1}^{N} |u_n|)^2 &= 1_{N\times 1}^T |A| 1_{N\times 1} \\ &= tr(1_{N\times N}|A|) = tr(1_{N\times N}B) \end{aligned}} \tag{2.6}$$

Here, it can be seen that appending the original objective function with the trace of the product of a $N \times N$ matrix of ones and the absolute value of A, denoted B, will produce the same result as would be achieved using the one-norm squared. After combining the above result with the result from the SDR the objective function, can now be rewritten as:

$$\boxed{\begin{aligned} \min_{\mathbf{A}\in\mathbb{C}^{N\times N}} \; & tr(\mathbf{A}) + tr(1_{N\times N}\mathbf{B}) \\ &= tr(\mathbf{A} + 1_{N\times N}\mathbf{B}) \end{aligned}} \tag{2.7}$$

In this form, the objective function is both convex and also penalizes the use of additional, unnecessary, transducer elements. However, nothing in the problem statement forces B to be the absolute value of A. Furthermore, the inclusion of an absolute value statement in the objective function would bring the objective function out of standard form. Thus, it is necessary to utilize Sylvester's Criterion for positive semidefiniteness [20]. This equality allows us to embed the absolute value relationship between A and B within the constraints that define the convex set over which an optimal solution will be sought. For a 2×2 matrix, the criterion states that a matrix is positive semidefinite if, and only if, the product of the elements on the diagonal is greater than or equal to that of the elements on the counter diagonal. Thus, the absolute value constraint can be

achieved with the addition of the constraints $B(i,j)^2 >= \Re(A(i,j))^2 + \Im(A(i,j))^2$, in the form of the following Linear Matrix Inequality (LMI) constraints:

$$\boxed{\begin{bmatrix} B(i,j) - \Re(A(i,j)) & \Im(A(i,j)) \\ \Im(A(i,j)) & B(i,j) - \Re(A(i,j)) \end{bmatrix} \succcurlyeq 0} \tag{2.8}$$

Here, **i** and **j** each have values $\{1, ..., N\}$. Now, the problem can be written as a convex optimization problem as follows:

$$\boxed{\begin{aligned} \min_{\mathbf{A} \in \mathbb{C}^{N \times N}} \quad & tr(\mathbf{A} + \lambda \mathbf{1}_{N \times N} \mathbf{B}) \\ \text{s.t.}: \quad & tr(\mathbf{A}\mathbf{Q}_i) \geq \mathbf{p}_{ti}, \quad i = 1, \ldots, L \\ & tr(\mathbf{A}\mathbf{F}_j) \leq \mathbf{p}_{rj}, \quad j = 1, \ldots, M \\ & \mathbf{A} \succcurlyeq 0 \\ & \begin{bmatrix} B(i,j) - \Re(A(i,j)) & \Im(A(i,j)) \\ \Im(A(i,j)) & B(i,j) - \Re(A(i,j)) \end{bmatrix} \succcurlyeq 0 \end{aligned}} \tag{2.9}$$

The MATLAB toolboxes `SeDuMi` [34] and `YALMIP` [35] can now be used to solve the problem. Elements corresponding to zeros on the diagonal of the optimal A are removed, leaving a smaller array of transducers. This solution does not correspond to the minimum power solution due to the influence of the one-norm, but it does produce a smaller transducer array that is composed of elements capable of producing a high therapeutic gain [20]. A modified version of the original LPD problem is now run, where in place of the original N elements, only the elements left on during sparsity induction are considered. The LPD algorithm is now able to focus the array, avoiding the influence of the one-norm while also utilizing the sparsity that it induced. As λ approaches ∞, the number of transducer elements tends towards the minimum feasible number. Alternatively, as λ approaches 0, the influence of the one-norm becomes increasingly negligible, and the solution converges towards the solution yielded by the original, unaltered LPD method [20].

2.4 Relaxation of Iterative Sparsity Inducing Terms

Element selection can also be conducted using an iteratively reweighed penalty matrix, in addition to the use of the one-norm squared [20]. The iterative process involves minimizing the trace of the product of a penalty matrix, Z, and the absolute value of A, again denoted B. Once again the absolute value constraint is achieved using the aforementioned LMI constraints. The penalty matrix is the product of the vector multiplication zz^T, where z is a $N \times 1$ vector containing positive penalties corresponding to each of the transducer elements. The values of Z are recalculated at the beginning of each iteration, so that they are inversely proportional to the magnitude of their corresponding element in the optimal A during the previous iteration. The objective function can

now be realized in convex form using the following equivalencies [20]:

$$\boxed{\begin{aligned}\sum_{i=1}^{N}\sum_{j=1}^{N} Z_{i,j}|A_{i,j}| &= tr(Z|A|)\\ &= tr(ZB)\end{aligned}} \tag{2.10}$$

The optimization problem can now be rewritten in convex form as:

$$\boxed{\begin{aligned}\min_{\mathbf{A}\in\mathbb{C}^{N\times N}} \quad & tr(Z^{(r)}B^{(r)})\\ \text{s.t.}: \quad & tr(\mathbf{A}^{(r)}\mathbf{Q}_i) \geq \mathbf{p}_{ti}, \quad i=1,\ldots,L\\ & tr(\mathbf{A}^{(r)}\mathbf{F}_j) \leq \mathbf{p}_{rj}, \quad j=1,\ldots,M\\ & \mathbf{A}^{(r)} \succcurlyeq 0\\ & LMI\ Constraints \succcurlyeq 0\end{aligned}} \tag{2.11}$$

Here, r denotes the r-th iteration of the optimization problem. During the first iteration, Z is initialized to be a $N \times N$ matrix of ones. After each iteration, the penalty matrix is updated so that each of its elements is inversely proportional to the magnitude of the corresponding element in A during the previous iteration. The purpose of this is to apply additional pressure for low magnitude elements to be switched off in subsequent iterations. Prior to the beginning of each iteration, Z is recalculated using the following equation, as was done in [20]:

$$\boxed{Z_{i,j}^{(r+1)} = 1/(B_{i,j}+\epsilon)} \tag{2.12}$$

Here, ϵ is a very small number used to ensure stability in the event that an element of B is close to zero. Similar to the noniterative method, elements corresponding to a 0 on the diagonal of A are considered to be off. Once an element is turned off during an iteration, its penalty in future iterations will be very large, forcing it to zero in all subsequent iterations. Accordingly, it is removed from subsequent iterations, allowing for the faster convergence of those iterations. The process of iteratively performing the optimization and then updating the penalty weight matrix is carried out until either a prescribed minimum number of elements are removed, or a predetermined maximum number of iterations has occurred. In the case of the process terminating due to the number of transducer elements being shutoff exceeding a predetermined number, the number of removed transducers is also compared to a predetermined maximum. In the event that the number of removed elements is below this threshold, the process terminates. Conversely, if the number of removed transducers exceeds the threshold the penalty matrix from the previous iteration is utilized

to create a new objective function of the following form [20]:

$$\begin{aligned} \min_{\mathbf{A}\in\mathbb{C}^{N\times N}} \quad & tr(A + \lambda^{(r)} Z^{(r)} B^{(r)}) \\ \text{s.t.}: \quad & tr(\mathbf{A}^{(r)}\mathbf{Q}_i) \geq \mathbf{p}_{ti}, \quad i = 1, \ldots, L \\ & tr(\mathbf{A}^{(r)}\mathbf{F}_j) \leq \mathbf{p}_{rj}, \quad j = 1, \ldots, M \\ & \mathbf{A}^{(r)} \succcurlyeq 0 \\ & LMI\ Constraints \end{aligned} \tag{2.13}$$

Here, λ is used to determine the relative importance of the sparsity inducing term during each iteration. After each iteration, the number of removed elements is again compared to the minimum and maximum removal thresholds. If the number of removed elements is too high, the value of λ is reduced. Conversely, if the number of removed elements is too low, the value of λ is increased. This process is repeated until the number of removed elements falls within the predetermined range. Again, the solution yielded by the sparsity inducing technique is not the minimum power solution. Accordingly, it is once again necessary to perform the LPD method on the reduced size transducer array.

Chapter 3

Methods

The model used to evaluate the effectiveness of the focusing consisted of a target that is obscured by four ribs within an inhomogeneous ROI. In the simulations, a spherical transducer array of 64 elements was focused onto the target point(s), as shown in Fig. 2.1.

The center of the ribs are vertically spaced 16 mm away from each other, and each rib measures 9.25 mm in diameter. The center of the array is a lateral distance of 55 mm and 100 mm away from the ribs and the target, respectively. Additionally, the tissue medium and ribs are assumed to have densities of 1090 and 1800 (kg/m^3), specific heats of 3540 and 1300 $(J/kg^{\circ}C)$, thermal conductivities of 0.52 and 0.32 $(Wm^{-1}/^{\circ}C)$, speed of sounds of 1500 and 2800 (m/s), and attenuations of .94 and 4 (dB/cm/MHz), respectively.

Numerical methods are used to model the field intensity and temperature rise throughout the ROI as functions of both position and time at the nodes of the discretized ROI. The model uses partial differential equations describing the acoustic and thermal propagation within the ROI. A finite difference approximation is used to obtain values for the partial derivatives of these functions throughout the ROI as functions of their values at the neighboring grid points. The finite difference equations are applied at the boundary points as well as the interior nodes by using a Perfectly Matching Layer (PML) that absorbs the HIFU beam [36] to extend the solution beyond the ROI.

3.1 Acoustic Model

The propagation of acoustic waves in the tissue-like medium of the ROI is described by the wave equation that was developed in [37]. The wave equation is shown in equation 3.1.

$$\boxed{\begin{aligned}\frac{\partial \mathbf{v}}{\partial t} &= \frac{-1}{\rho}\nabla p \\ \frac{\partial p}{\partial t} &= -\rho.c^2\nabla.\mathbf{v} + \alpha p\end{aligned}} \tag{3.1}$$

$$\boxed{\begin{aligned}s_\xi \frac{\partial}{\partial t} v_\xi + (h\sigma)_\xi v_\xi &= -\frac{1}{p}\nabla p \\ s_\xi \frac{\partial}{\partial t} p &= -h\nabla v - (s_\xi \gamma c^2 + (h\sigma)_\xi)p\end{aligned}} \tag{3.2}$$

Here, v, p, α and c, are the particle velocity, pressure, attenuation coefficient, and speed of sound, respectively. By coupling these two equations, a second order partial differential equation is obtained, as shown below [37]:

$$\boxed{\frac{1}{c^2}\frac{\partial^2 p}{\partial^2 t} = p\nabla.p^{-1}\nabla p - \gamma\frac{\partial p}{\partial t}} \tag{3.3}$$

The previous set of equations that yielded the differential equation when coupled is modified by using stretch coordinates and replacing ∇ with ∇_g, as shown in equation 3.4. This gives the set of equations shown below [37]:

$$\boxed{\begin{aligned}s_\xi \frac{\partial}{\partial t} v_\xi + (h\sigma)_\xi v_\xi &= -\frac{1}{p}\nabla p \\ s_\xi \frac{\partial}{\partial t} p &= -h\nabla v - (s_\xi \gamma c^2 + (h\sigma)_\xi)p\end{aligned}} \tag{3.4}$$

Here, $(h\sigma)_\xi$ is the loss in the perfectly matched layer (PML) and s_ξ is a scaling factor. These equations are used for the entire computational domain, with $s_\xi = 1$ and $(h\sigma)_\xi = 0$ for the interior of the domain. Spatial and temporal derivatives are approximated using a Taylor series expansion for each node in the computational grid. The spatial and temporal dimensions are both comprised of uniformly spaced nodes. The PML applied to the border of the edge of the domain eliminates reflections from the outer boundary. The pressure within the domain can now be described with the equation [37]:

$$\boxed{\begin{aligned}&s_\xi[p(j_x, j_y, j_z, n+1) - v_x(j_x, j_y, j_z, n)]\nabla t \\ &+(s_\xi \beta c^2 + (h\sigma)_\xi) + [p(j_x, j_y, j_z, n+1) \\ &+p(j_x, j_y, j_z, n)]/2 \\ &= -\frac{h}{\nabla \xi}[v(j_x+1, j_y, j_z, n) - v(j_x, j_y, j_z, n)]\end{aligned}} \tag{3.5}$$

The time stepping equation for pressure is approximately [37]:

$$\begin{aligned} p(j_x, j_y, j_z, n+1) = Cp(j_x, j_y, j_z, n) \\ +D[v_x(j_x+1, j_y, j_z, n) - v_x(j_x, j_y, j_z, n)] \end{aligned} \tag{3.6}$$

Here, C and D are described by equation 3.7. The PML consists of $L = 40$ cells. These cells have increasingly quadric attenuations as the outer boundary is approached. This is described by equation 3.8 [37].

$$\begin{aligned} C &= \frac{s_\xi/\nabla t - (s_\xi \gamma c^2 + (h\sigma)_\xi)/2}{s_\xi/\nabla t + (s_\xi \gamma c^2 + (h\sigma)_\xi)/2} \\ D &= -\frac{h}{\nabla \xi [s_\xi/\nabla t + (s_\xi \gamma c^2 + (h\sigma)_\xi)/2]} \end{aligned} \tag{3.7}$$

$$(h\sigma)_\xi(j_\xi) = \frac{(L - .5 - j_\xi)^q}{(L-.5)^q}(h\sigma)_{\xi,max} p \tag{3.8}$$

3.2 Thermal Model

The bioheat transfer equation used in the modeling is shown in equation 3.9 [37]. Here, T, T_b, ρ, C_t, C_b, k, Q, and W_b are the tissue temperature (°C), arterial blood temperature °C, tissue density (kg/m^3), specific heat of tissue ($J/kg.°C$), specific heat of blood, thermal conductivity of the tissue ($W/m°C$), applied transducer intensity (W/m^3), and perfusion parameter ($kg/m^3 s$), calculated using the complex pressures at each grid point, respectively.

$$\rho C_t \frac{\partial T}{\partial t} = \nabla k \nabla T - W_b C_b (T - T_b) + Q \tag{3.9}$$

A forward difference was used for the time derivative, while a backward difference was used for the spatial derivative. A centered second spatial derivative was used. This is shown in [37]:

$$\begin{aligned} \rho C_T \frac{T^{n+1}_{i,j,l} - T^n_{i,j,l}}{k\Delta t} =& \frac{T^n_{i+1,j,l} - T^n_{i,j,l} + T^n_{i-1,j,l}}{\Delta x} \\ &+ \frac{T^n_{i,j+1,l} - T^n_{i,j,l} + T^n_{i,j-1,l}}{\Delta y} + \frac{T^n_{i,j,l+1} - T^n_{i,j,l} + T^n_{i,j,l-1}}{\Delta z} \\ &- \frac{w_b C_b (T_a - T^n_{i,j,l}) + Q}{k} \end{aligned} \tag{3.10}$$

This method produces numerical errors on the order of Δt and $\Delta \xi$. Stability is ensured by adhering to the Courant, Friedrichs and Lewy (CFL) condition for the convergence of a difference approximation.

Chapter 4

Results

4.1 Simulation Results and Discussion

The simulations used to validate the algorithms proposed in this paper were performed using a spherical 1 MHz phased-array with 64 elements, similar to [17]. The acoustic simulations had a grid spacing of 0.15 mm, which is one-tenth of the emitted ultrasound waves' wavelength while traveling through water. A 5 second transducer excitation period was utilized during the thermal simulations. During the noniterative sparsity induction, λ had a value of 8×10^5. With this value of λ, 18 elements were removed from consideration during the subsequent HIFU focusing using the LPD method. The iterative method of sparsity induction, was able to remove 23 elements. The iterative method was able to remove more elements from consideration because the iteratively reweighed penalty matrix harshly penalized low magnitude excitation transducers, leading to their eventual exclusion from the treatment. As can be seen from Fig. 4.5 and Fig. 4.6, both elements favored the removal of elements that were aligned with the explicitly protected critical rib points.

Fig. 4.1 and Fig. 4.2 show the field intensity profiles achieved using each of the methods in the focal and rib planes, respectively. The resulting temperature rise profiles that occurred during the treatments are shown in Fig. 4.3 and Fig. 4.4. Due to the low-pass nature of the BHTE used for the simulations, the simulated temperature rise profiles are smoothed versions of those that would actually occur during treatment. Fig. 4.2 shows the field intensity in the rib plane as a whole is less for either of the sparse LPD methods than for the shadowing method. Due to the resulting intensity profiles in the rib plane, the sparse LPD methods produced temperature rise profiles in this plane that were lower in magnitude. Fig. 4.2 shows that each of the methods favored ultrasound transmission through the unprotected intercostals, rather than through the critical rib points. However, Fig. 4.4 reveals that while the sparse LPD methods have high intensities within the intercostals, the temperature rise in these regions, relative to the temperature rise seen in the intercostals when using the shadowing method, is low meaning that these areas have a reduced

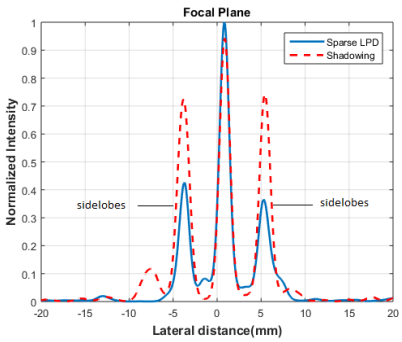

Figure 4.1: Simulated field intensity pattern in the focal plane for the sparse LPD method (solid line), ray tracing (shadowing) method (dashed line).

risk of being damaged during the administration of the HIFU treatment. This is of particular importance because these regions are not protected in the problem statement, exposing them to an elevated risk of developing burns. Despite the intercostals having a higher specific heat than the ribs, meaning that it takes a greater amount of energy to raise their temperature, the high energy deposition upon these regions in can be dangerous if left unchecked. While the shadowing method leaves no recourse, other than lowering the magnitude of the excitation of the transducer array, in the event that the intercostals overheat, the optimization based approach of the sparse LPD methods allow for additional constraints to be placed on the heating of these regions, at the cost of increased computational complexity. However, the problem statement of the LPD method allows for a benign amount of power deposition onto the ribs, rather that trying to minimize it like the shadowing method, reducing the likelihood of requiring additional constraints to ensure a safe treatment administration.

Fig. 4.1 shows that utilization either sparse LPD method resulted in a higher focal intensity, while also reducing the size of the side lobes that occurred in the focal plane. As a result, the target point has a higher temperature rise, while the surrounding tissue has a lower temperature rise, as seen in Fig. 4.3. Accordingly, the treatment would more likely lead to the successful removal of the tissue being targeted, while also exposing the patient to less risk of developing burns in other parts of the ROI. The combination of the higher focal gain and lower rib plane power deposition show that the algorithms proposed in this paper have a higher treatment efficacy than the shadowing method. The methods outlined in this paper are able to outperform the shadowing method by more effectively utilizing the degrees of freedom both during the element selection phase and the subsequent focusing. Accordingly, the sparse LPD methods are able to achieve the advantages enjoyed by the ray tracing method, such as reserving transducers for parallel use in other processes, while providing better treatment efficacy.

The two variations of the LPD method proposed in this paper sought to limit the number of transducers utilized by using the one-norm squared and an iteratively reweighed penalty matrix to optimally induce sparsity by minimizing an objective function that punished the use of additional elements. Conversely, the shadowing method used a more intuitive approach by relying only upon basic analysis of the geometry of the ROI during element section [5]. As a result, the sparse LPD methods were able to better select which elements to utilize for the treatment, resulting in a higher treatment efficacy.

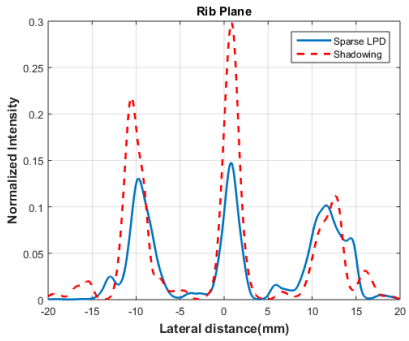

Figure 4.2: Simulated field intensity pattern rib plane for the sparse LPD method (solid line), ray tracing (shadowing) method (dashed line).

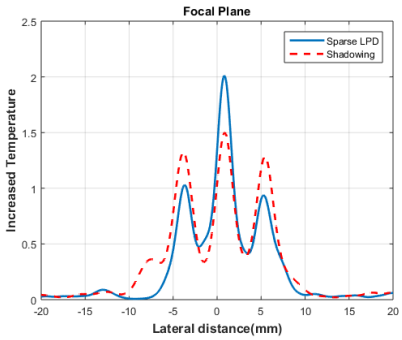

Figure 4.3: Simulated temperature rise pattern at the focal plane for the sparse LPD method (solid line), ray tracing (shadowing) method (dashed line).

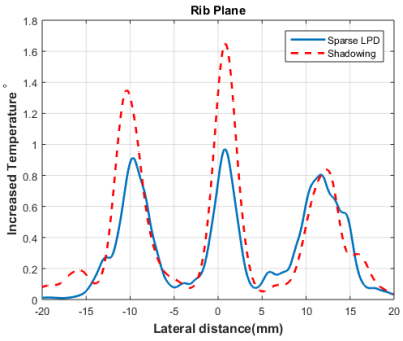

Figure 4.4: Simulated temperature rise pattern in the rib plane for the sparse LPD method (solid line), ray tracing (shadowing) method (dashed line).

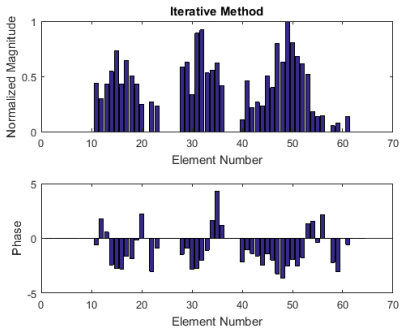

Figure 4.5: Optimal transducer excitation magnitude (top) and phase (bottom) achieved using the LPD method after iteratively forcing sparsity.

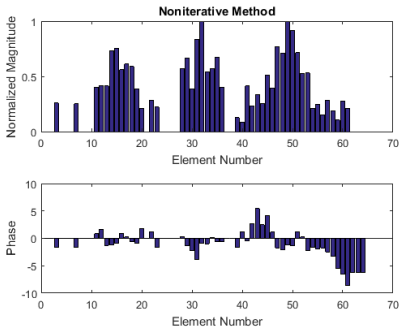

Figure 4.6: Optimal transducer excitation magnitude (top) and phase (bottom) achieved using the LPD method after noniteratively forcing sparsity.

4.2 Conclusion

New techniques for HIFU element selection that built upon the LPD method by using the one-norm squared as a surrogate element counter were introduced in this paper and compared to the shadowing method, a previously known sparse algorithm. The simulation results presented in this paper validate the use of the one-norm squared as an appropriate substitute for the intuitive approach employed by the shadowing method for element selection. By accounting for diffraction and interference, the optimization based algorithms were able to select the elements that deposited energy with the most therapeutic benefit for inclusion during HIFU treatment administration. Accordingly, the optimization based approaches were able to achieve treatments that were both safer and more effective than their geometry based counterpart.

Bibliography

[1] C. M. Tempany, E. A. Stewart, N. McDannold, B. J. Quade, F. A. Jolesz, and K. Hynynen. MR imaging–guided focused ultrasound surgery of uterine leiomyomas: a feasibility study. *Radiology*, 226(3):897–905, 2003.

[2] N. Sanghvi, F. J. Fry, R. Bihrle, R. Foster, M. Phillips, J. Syrus, A. Zaitsev, and C. Hennige. Noninvasive surgery of prostate tissue by high-intensity focused ultrasound. *IEEE Transactions on Ultrasonics, Ferroelectrics, and Frequency Control*, 43(6):1099–1110, 1996.

[3] A. H. Chan, V. Y. Fujimoto, D. E. Moore, R. W. Martin, and S. Vaezy. An image-guided high intensity focused ultrasound device for uterine fibroids treatment. *Medical physics*, 29(11):2611–2620, 2002.

[4] I. A. Shehata. Treatment with high intensity focused ultrasound: secrets revealed. *European journal of radiology*, 81(3):534–541, 2012.

[5] P. Gélat, G. Ter Haar, and N. Saffari. The optimization of acoustic fields for ablative therapies of tumours in the upper abdomen. *Physics in medicine and biology*, 57(24):8471, 2012.

[6] Y. Y. Botros, E. S. Ebbini, and J. L. Volakis. Two-step hybrid virtual array ray (VAR) technique for focusing through the rib cage. *IEEE transactions on ultrasonics, ferroelectrics, and frequency control*, 45(4):989–1000, 1998.

[7] J.-F. Aubry, M. Pernot, F. Marquet, M. Tanter, and M. Fink. Transcostal high-intensity-focused ultrasound: ex vivo adaptive focusing feasibility study. *Physics in medicine and biology*, 53(11):2937, 2008.

[8] M. Fink. Time reversal of ultrasonic fields. I. Basic principles. *IEEE transactions on ultrasonics, ferroelectrics, and frequency control*, 39(5):555–566, 1992.

[9] F. Wu, J.-L. Thomas, and M. Fink. Time reversal of ultrasonic fields. Il. Experimental results. *IEEE transactions on ultrasonics, ferroelectrics, and frequency control*, 39(5):567–578, 1992.

[10] C. Prada, J.-L. Thomas, and M. Fink. The iterative time reversal process: Analysis of the convergence. *The Journal of the Acoustical Society of America*, 97(1):62–71, 1995.

[11] J.-L. Thomas and M. A. Fink. Ultrasonic beam focusing through tissue inhomogeneities with a time reversal mirror: application to transskull therapy. *IEEE Transactions on Ultrasonics, Ferroelectrics, and Frequency Control*, 43(6):1122–1129, 1996.

[12] M. Tanter, J.-L. Thomas, and M. Fink. Focusing and steering through absorbing and aberrating layers: Application to ultrasonic propagation through the skull. *The Journal of the Acoustical Society of America*, 103(5):2403–2410, 1998.

[13] M. Tanter, M. Pernot, J.-F. Aubry, G. Montaldo, F. Marquet, and M. Fink. Compensating for bone interfaces and respiratory motion in high-intensity focused ultrasound. *International Journal of Hyperthermia*, 23(2):141–151, 2007.

[14] P. Gelat, G. Ter Haar, and N. Saffari. Scattering of the field of a multi-element phased array by human ribs. In *Journal of Physics: Conference Series*, volume 353, page 012010. IOP Publishing, 2012.

[15] P. Gélat, G. Ter Haar, and N. Saffari. Modelling of the acoustic field of a multi-element HIFU array scattered by human ribs. *Physics in medicine and biology*, 56(17):5553, 2011.

[16] S. Bobkova, L. Gavrilov, V. Khokhlova, A. Shaw, and J. Hand. Focusing of high-intensity ultrasound through the rib cage using a therapeutic random phased array. *Ultrasound in medicine & biology*, 36(6):888–906, 2010.

[17] M. K. I. Almekkawy. Optimization of focused ultrasound and image based modeling in image guided interventions. 2014.

[18] M. Almekkawy, D. McMahon, H. Alqarni, and J. He. Optimization of transcostal phased-array refocusing using sparse semidefinite relaxation method. In *Engineering in Medicine and Biology Society (EMBC), 2017 39th Annual International Conference of the IEEE*, pages 1449–1452. IEEE, 2017.

[19] S. Boyd and L. Vandenberghe. *Convex optimization*. Cambridge university press, 2004.

[20] O. Mehanna, N. D. Sidiropoulos, and G. B. Giannakis. Multicast beamforming with antenna selection. In *Signal Processing Advances in Wireless Communications (SPAWC), 2012 IEEE 13th International Workshop on*, pages 70–74. IEEE, 2012.

[21] J. R. Ballard, A. J. Casper, Y. Wan, and E. S. Ebbini. Adaptive transthoracic refocusing of dual-mode ultrasound arrays. *IEEE Transactions on Biomedical Engineering*, 57(1):93–102, 2010.

[22] E. S. Ebbini and C. A. Cain. Multiple-focus ultrasound phased-array pattern synthesis: optimal driving-signal distributions for hyperthermia. *IEEE transactions on ultrasonics, ferroelectrics, and frequency control*, 36(5):540–548, 1989.

[23] Z.-Q. Luo, N. D. Sidiropoulos, P. Tseng, and S. Zhang. Approximation bounds for quadratic optimization with homogeneous quadratic constraints. *SIAM Journal on optimization*, 18(1):1–28, 2007.

[24] P. Tseng. Further results on approximating nonconvex quadratic optimization by semidefinite programming relaxation. *SIAM Journal on Optimization*, 14(1):268–283, 2003.

[25] Y. Nesterov, H. Wolkowicz, and Y. Ye. Semidefinite programming relaxations of nonconvex quadratic optimization. *Handbook of semidefinite programming*, pages 361–419, 2000.

[26] N. D. Sidiropoulos, T. N. Davidson, and Z.-Q. Luo. Transmit beamforming for physical-layer multicasting. *IEEE Transactions on Signal Processing*, 54(6):2239–2251, 2006.

[27] R. Seip, P. VanBaren, and E. S. Ebbini. Dynamic focusing in ultrasound hyperthermia treatments using implantable hydrophone arrays. *IEEE transactions on ultrasonics, ferroelectrics, and frequency control*, 41(5):706–713, 1994.

[28] J.-F. Aubry, M. Pernot, F. Marquet, M. Tanter, and M. Fink. Transcostal high-intensity-focused ultrasound: ex vivo adaptive focusing feasibility study. *Physics in medicine and biology*, 53(11):2937, 2008.

[29] C. Dorme and M. Fink. Ultrasonic beam steering through inhomogeneous layers with a time reversal mirror. *IEEE transactions on ultrasonics, ferroelectrics, and frequency control*, 43(1):167–175, 1996.

[30] E. Karipidis, N. D. Sidiropoulos, and Z.-Q. Luo. Quality of service and max-min fair transmit beamforming to multiple cochannel multicast groups. *IEEE Transactions on Signal Processing*, 56(3):1268–1279, 2008.

[31] K. T. Phan, S. A. Vorobyov, N. D. Sidiropoulos, and C. Tellambura. Spectrum sharing in wireless networks via QoS-aware secondary multicast beamforming. *IEEE Transactions on signal processing*, 57(6):2323–2335, 2009.

[32] O. Mehanna, N. D. Sidiropoulos, and G. B. Giannakis. Joint multicast beamforming and antenna selection. *IEEE Transactions on Signal Processing*, 61(10):2660–2674, 2013.

[33] E. J. Candes, M. B. Wakin, and S. P. Boyd. Enhancing sparsity by reweighted 1 minimization. *Journal of Fourier analysis and applications*, 14(5):877–905, 2008.

[34] J. F. Sturm. Using SeDuMi 1.02, a MATLAB toolbox for optimization over symmetric cones. *Optimization methods and software*, 11(1-4):625–653, 1999.

[35] J. Lofberg. YALMIP: A toolbox for modeling and optimization in MATLAB. In *Computer Aided Control Systems Design, 2004 IEEE International Symposium on*, pages 284–289. IEEE, 2004.

[36] Q.-H. Liu and J. Tao. The perfectly matched layer for acoustic waves in absorptive media. *The Journal of the Acoustical Society of America*, 102(4):2072–2082, 1997.

[37] M. K. Almekkaway, I. A. Shehata, and E. S. Ebbini. Anatomical-based model for simulation of HIFU-induced lesions in atherosclerotic plaques. *International Journal of Hyperthermia*, 31(4):433–442, 2015.

Academic Vita
Daniel F. McMahon

142 S. Allen Street, University Park, PA 16801
Cell: 412-706-2279; **Email:** dfm5128@psu.edu

Education

The Pennsylvania State University, Schreyer Honors College
Major: Electrical Engineering; **Concentration:** Signal Processing and Computer Engineering
Minor: Mathematics
Expected Graduation Date: December 2017

- Dean's List: 8 Semesters
- Relevant Courses: Computer Vision; Digital Design; Computer Organization and Design; Continuous Time Signal Processing; Discrete Time Signal Processing; Design Process
- Recipient: Department of Electrical Engineering General Scholarship
- Recipient: C. B. Holt Jr. Memorial Scholarship

Technical Experience

Researcher: therapeutic ultrasound, under direction of Penn State's Dr. Almekkawy, Professor of Engineering: 05/2016 to Present

Coauthored: the conference paper, "Sparse Optimization of Transcostal Phased-array Refocusing Using the Semidefinite Relaxation Method", accepted for presentation and subsequent publication at the IEEE EMBC 2017 Conference

Researched high intensity focused ultrasound as follows:

- Adapted a sparsity algorithm used for broadcast antenna selection to be used for ultrasound transducer selection using MATLAB;
- Wrote an iterative sparsity algorithm for ultrasound transducer selection in MATLAB;
- Contributed to a MATLAB script that iteratively solves the inverse problem to determine the acoustic properties of the area targeted by the ultrasound array;

Technical Skills

MATLAB; LabVIEW; C++; Verilog; Python

Sample of Completed Projects

Realization of super magnet control system using LabVIEW
Instantiation of Optical Theremin using LabVIEW
Instantiation of MIPS Architecture using Verilog

Activities

Pediatric Cancer Fundraiser: Ohana FTK (Alternative Funds Captain)
Math Club